Multifunctional derivatives of dimethoxy-substituted triphenylamine containing different acceptor moieties

Dalius Gudeika, Arturs Bundulis, Safia Benhattab, Marwa Ben Manaa, Nicolas Berton, Johann Bouclé, François Tran Van, Bruno Schmaltz, Dmytro Volyniuk, Martins Rutkis, et al.

Multifunctional derivatives of dimethoxy-substituted triphenylamine containing different acceptor moieties

Dalius Gudeika[a,d], Arturs Bundulis[d], Safia Benhattab[b], Marwa Ben Manaa[b], Nicolas Berton[b], Johann Bouclé[c], François Tran Van[b], Bruno Schmaltz[b], Dmytro Volyniuk[a], Martins Rutkis[d], Juozas V. Grazulevicius[a†]

[a] *Department of Polymer Chemistry and Technology, Kaunas University of Technology, Radvilenu pl. 19, LT- 50254, Kaunas, Lithuania;*

[b] *Université de Tours, Laboratoire de Physico-Chimie des Matériaux et des Electrolytes pour l'Energie (PCM2E), EA 6299, Parc de Grandmont, F-37200 Tours, France;*

[c] *Institut XLIM UMR 7252, Université de Limoges/CNRS, 123 av. A. Thomas, F-87060 Limoges, France;*

[d] *Institute of Solid State Physics, University of Latvia, 8 Kengaraga St., Riga LV-1063, Latvia;*

Corresponding author. E-mail address: juozas.grazulevicius@ktu.lt (Juozas Vidas Gražulevičius).

Abstract

Two compounds, having dimethoxy-substituted triphenylamino groups and fragments of cyanoacrylic acid or rhodanine-3-acetic acid were prepared and characterized. Their optical, photophysical, thermal, electrochemical, photoelectrical and nonlinear optical properties were investigated. Both derivatives

showed ability of glass-formation with glass transition temperatures of 83 and 61 ºC. They showed comparable ionization potential values of *ca.* 5.20 eV. The compounds showed Kerr and two photon absorption effects. The dye containing a rhodanine-3-acetic acid fragment, namely 2-((E)-5-(4-(diphenylamino)benzylidene)-tetrahydro-4-oxo-2-thioxothiophen-3-yl)acetic acid, exhibited a promising power conversion efficiency of 2.09% in dye-sensitized solar cells using the spiro-OMeTAD as hole transporting compound.

Keywords: dimethoxy-substituted triphenylamine, cyanoacrylic acid, rhodanine-3-acetic acid, dye-sensitized solar cell, two photon absorption effect, Kerr effect.

Introduction

In recent years, the investigation on solar cells using organic semiconducting derivatives has made considerable advance [1]. Among the promising photovoltaic technologies, dye-sensitized solar cells (DSSCs) have received much attention recently due to their low cost and relatively high efficiency [2]. Generally, DSSCs are based on a photoelectrode sensitized by a dye [3], where photo-induced electron transfers occur [3]. A counter electrode and a liquid electrolyte complete the cell [4]. High efficiencies of ca. 13% were reached by employing a metal complex redox couple (namely Co(II/III)tris(bipyridyl)) and organic dyes [4]. Hole transporting materials (HTM) were successfully applied in solid state dye-sensitized solar cells (ssDSSCs) which allow to avoid potential leakage problems associated with the volatile nature of the liquid electrolyte [5,6]. During the last few years, spiro-OMeTAD has shown ascending performance when related with organic dyes such as Y123 (7.2%) [7] and D102 (4.2%) [8].

However, the synthesis of these dyes requires a multistep procedures which are costly and time consuming [9].

Most conventional organic dyes possess the push-pull structure of "donor-conjugated bridge-acceptor". Typically, organic dyes used for efficient solar cells are required to afford intense and broad absorption in the visible spectral region. Aside from donor units, the electron acceptor plays a significant role in the performance control of DSSCs [10].

Recently, derivatives containing triphenylamino moieties as donor units have shown potential applications in photovoltaic devices [10]. Triphenylamino moiety is able to extend the light absorption capability of the dyes [11]. Moreover, triphenylamine is sustained as a perfect donor moiety in organic dyes, since it is able to demonstrate high hole-transporting and a perfect electron-donating capability [12]. Introducing an additional electron-donating moiety into derivative of triphenylamine can enhance charge separation, which result in high overall conversion efficiency [13]. Due to the certain peculiarities of the structure of triphenylamine, electron acceptor groups can be introduced. They can affect the molar extinction coefficients, absorption spectra, and the HOMO, LUMO energy levels of the derivatives. Rhodanine 3-acetic acid and cyanoacetic acid were introduced into triphenylamine-based dyes as acceptor moieties [14].

As demand for new nonlinear optical (NLO) materials for optical data storage [15], optical data processing [16] and other NLO applications grows, more and more researches are dedicated to study NLO properties of different materials. Organic NLO materials have attracted great interest due to possibility to tune NLO properties by varying molecular structure. Although vast number of papers has already been published regarding structure-properties relations of organic NLO materials [17,18,19], still there is lack of qualitative criteria to theoretically design organic molecules for NLO applications.

On the other hand, in order to further improve the characteristics of triphenylamine sensitized solar cells, deeper insight should be committed to the structure-property relationships of triphenylamine-based of dyes. In this paper, easily synthesized dyes based on dimethoxy-substituted triphenylamines were obtained by a Knoevenagel condensation. Two different dyes containing cyanoacrylic acid (compound **1**) and rhodanine-3-acetic acid (compound **2**) moieties as an electron acceptors were prepared. These dyes show interesting electronic and optoelectronic properties and, as we show, constitute potential candidates to be used in solid state dye sensitized solar cells based using the structure of FTO/TiO_2/Dye/Spiro-OMeTAD/Ag. In addition, we studied Kerr and two-photon absorption effects of the synthesized derivatives to understand how different acceptor groups influence NLO properties.

Results and discussion

Synthesis

The intermediate derivative (**II**) was prepared by formylation reaction of the derivative of triphenylamine (**I**). Compounds **1** and **2** were synthesyzed by Knoevenagel condensation of the formyl derivative of triphenylamine (**II**) with cyanoacrylic acid or rhodanine-3-acetic acid, respectively in DMF using zinc acetate dihydrate (Scheme 1). The chemical structures of **1** and **2** were proved by IR, ^{1}H NMR and ^{13}C NMR spectroscopies, mass spectrometry, elemental analysis. Derivatives are soluble in acetone, dichloromethane, THF, ethylacetate etc.

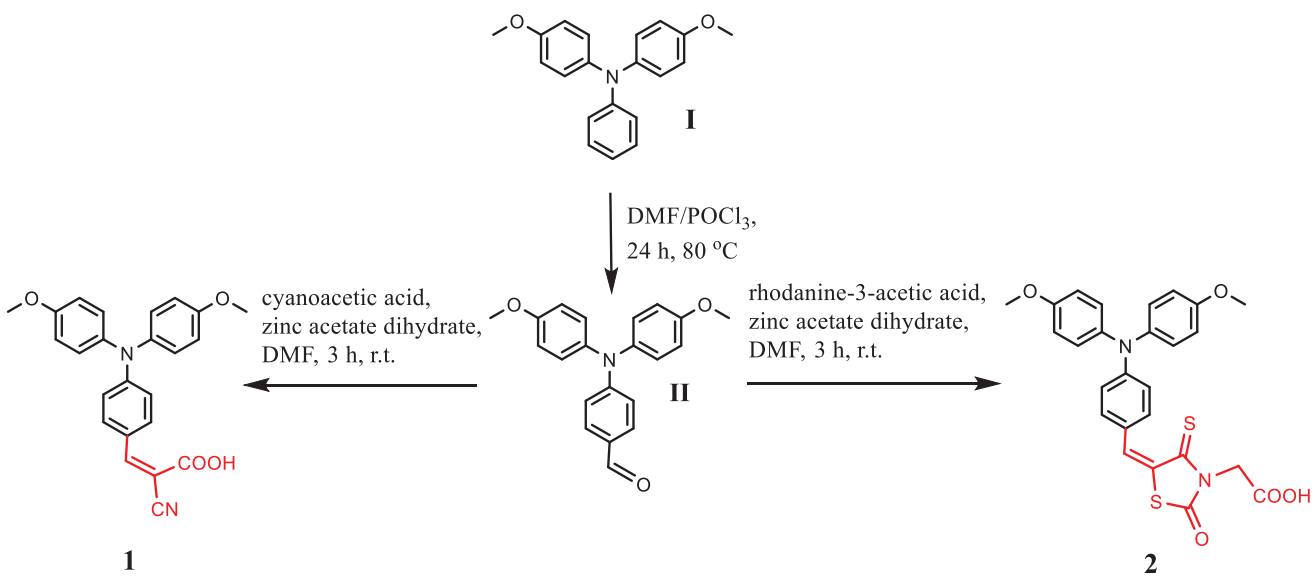

Scheme 1. Synthesis way to derivatives **1** and **2**.

Thermal properties

The thermal characteristics of **1** and **2** were obtained by differential scanning calorimetry (DSC) and thermogravimetric analysis (TGA). Derivatives **1**, **2** were obtained after the synthesis and purification as crystalline substances as confirmed by DSC. The DSC thermograms of **1** and **2** are shown in Fig. 1, Fig. S1. When the crystalline samples were heated in the first heating scan, the endothermic peaks due to melting were observed at 201 and 121 °C, respectively. When the melted samples were cooled down and heated again, glass transition temperatures were observed at 83 °C (for **1**) or 61 °C (for **2**). TGA revealed single-stage decomposition of compounds **1**, **2** (Fig. S1). Compound **1** showed considerably higher 5% weight loss temperature of 283 °C as compared with that of compound **1** (195 °C, Table 1). This observation can apparently be explained by the lower thermal stability of the rhodanine-3-acetic acid moiety relative to that of the fragment of cyanoacrylic acid. Higher thermal stability

of compound **1** can also be explained by the stronger intermolecular interaction in the solid state, which is evidenced by considerably higher melting point.

Table 1. Thermal characteristics of derivatives **1** and **2**.

Derivative	T_m, [°C]	T_g, [°C] (2nd heating)	$T_{ID-5\%}$, [°C]
1	201	83	283
2	121	61	195

T_g - glass transition point, T_m - melting point (10 °C/min, nitrogen atmosphere). $T_{ID-5\%}$ is 5% (20 °C/min under nitrogen).

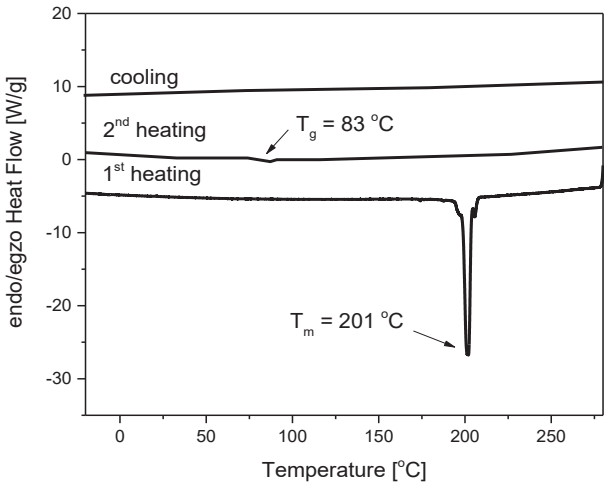

Figure 1. DSC thermograms of **1**.

Optical properties

UV absorption spectra of the dilute solutions of **1** and **2** in toluene (10^{-5} M) are shown in Fig. 2.

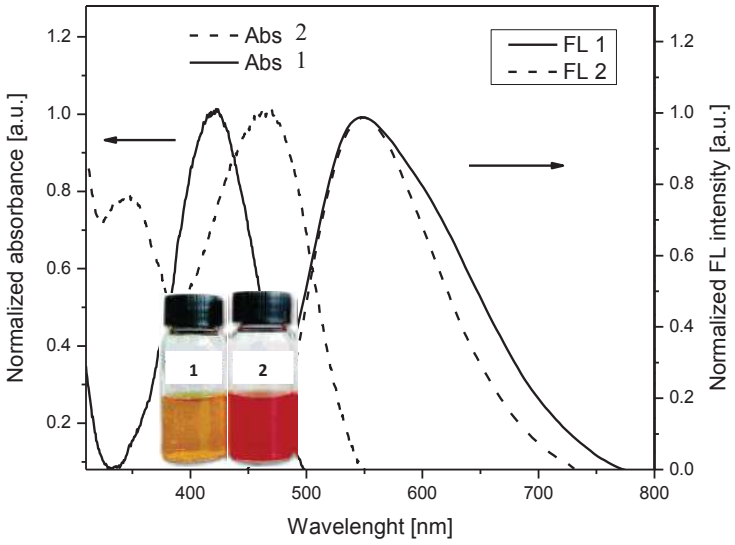

Figure 2. Normalized UV and FL spectra of dilute solutions of **1** and **2** in toluene at 298 K.

Absorption intensity maxima at 424 and 466 nm observed in UV spectra of the solutions of **1** and **2** can be assigned to an intramolecular charge transfer (ICT) between cyanoacrylic acid or rhodanine-3-acetic acid moieties and triphenylamino unit [20,21]. UV spectrum of the solution of compound **2** exhibited red-shift with respect of that of the solution of compound **1**. The solution of compound **1** having cyanoacrylic acid moiety exhibited higher molar extinction coefficients at the maximum absorption wavelength compared to those of compound **2** containing rhodanine-3-acetic acid fragment. The relatively high molar extinction coefficient of the solution of **1** (2.4×10^4 M^{-1} cm^{-1}) indicates its good ability for light harvesting. The optical band gap (E^g_{opt}) of the solution of **1** (2.28 eV) was found to be lower than that of the solution of **2** (2.52 eV, Table 2).

Table 2. UV and emission data of dilute solutions (10^{-5} M) of **1** and **2** in toluene.

Compound	λ_{max}[a], nm	ε[b] (10^4 $M^{-1}cm^{-1}$)	λ_{max}[c], nm	Φ_F[d], %	Stokes shift, nm	E_g^{op} /eV[e]
1	424	2.4	552	19.56	128	2.28
2	466	1.8	553	14.25	87	2.52

[a] Wavelength of absorption maximum. [b] ε is the extinction coefficient at λ_{max} of absorption. [c] Wavelength of photoluminescence emission maximum. [d] Fluorescence quantum yield. [e] $E_g^{op} = 1240/\lambda_{edge}$, where λ_{edge} is the wavelength of absorption edge in long wave direction.

The wavelengths of emission intensity maxima of the solutions of **1** and **2** were found to be close (552 and 553 nm, respectively). The Stokes shift of the solution of compound **1** (128 nm) was found to be considerably larger than that of the solution of **2** (87 nm). This observation can be attributed to the geometrically more relaxed structure of derivative **1** upon excitation [22]. The solutions of materials **1** and **2** showed relatively low fluorescence quantum yields (19.56 and 14.25%, respectively).

Frontier orbitals, photoelectrical and electrochemical properties

Electrochemical properties of derivatives **1** and **2** were investigated by cyclic voltammetry (CV) using their 1×10^{-6} M solutions in dichloromethane. CVs of the derivatives are present in Fig. 3a, Fig. S2. The onset oxidation potential *vs.* Fc together with the values of the electron affinity (EA_{CV}) and ionization potential (IP_{CV}) values are listed in Table 3.

Table 3. Electrochemical characteristics of derivatives **1** and **2**.

Derivative	E^{ox}_{onset} vs Fc /V[a]	IP_{CV} /eV[b]	EA_{CV} /eV[b]	IP_{PE} /eV[c]
1	0.43	5.23	-2.91	5.26
2	0.38	5.18	-2.70	5.29

[a] E^{ox}_{onset} is oxidation potential *vs.* Fc/Fc^{+}; [b] Ionization potential, electron affinity values estimated according to the equation $IP_{CV} = -(E^{ox}_{onset}+4.8)$; (where E^{ox}_{onset} is onset oxidation potential *vs.* the Fc^{+}/Fc); $EA_{CV} = -(|IP_{CV}|-E^{opt}_{g})$; [c] The values of ionization potentials (IP_{PE}).

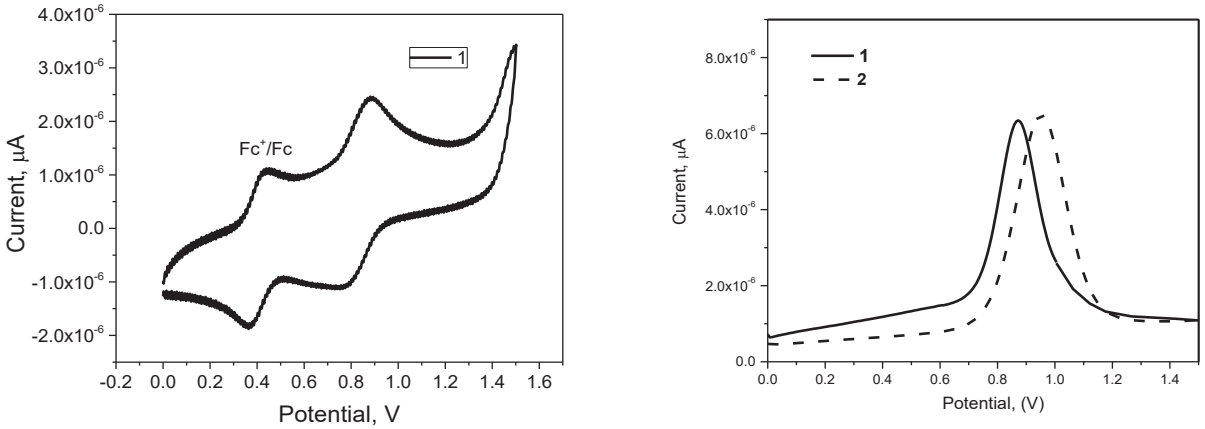

(a) (b)

Figure 3. (a) CV of **1** recorded in an inert atmosphere (100 mV/s vs Ag/Ag^{+}); (b) DPV curves of 1×10^{-6} M of compounds **1** and **2** in 0.1M Bu_4NBF_6/DCM electrolyte.

Oxidation of **1** and **2** is apparently related to the loss of electrons of TPA moiety, resulting in radical cations (one redox system) [23]. No reduction potentials were detected. Compound **1**

displayed a reversible oxidation potential in positive potential range at 0.43 V, whereas **2** showed a quasi-reversible oxidation potential at 0.38 V *vs* Fc. The presence of cyanoacrylic acid moiety in compound **1** resulted in slightly higher oxidation potential and thus slightly higher IP_{CV} value. The calculated EA_{CV} values for derivatives **1** and **2** were found to be -2.91 and -2.70 eV, respectively. In compound **1** the acceptor moiety apparently has stronger influence on the electrochemical properties as compared to **2**. For this reason, **1** showed higher IP_{CV} values than compound **2**. These results are in agreement with the results of density functional theory (DFT) calculations. The low energy absorption band of **1** appeared at lower energy than that of **2**.

Differential pulse voltammperometric (DPV [24]) spectra (Fig. 3b) of compounds **1** and **2** showed peaks of oxidation processes. The oxidation potential peak (0.87 V) of **1** having cyanoacrylic acid moiety was observed at a slightly higher potential compared to that of compound **2** containing rhodanine-3-acetic acid moiety (0.96 V).

To investigate electron distribution of the compounds, their structures were optimized using DFT calculations with Spartan 14 program [25]. The calculations were performed with the B3LYP under 6-31G (d) basis set. Fig. 4 presents the frontier molecular orbitals of the compounds.

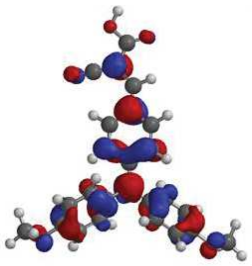

1 HOMO

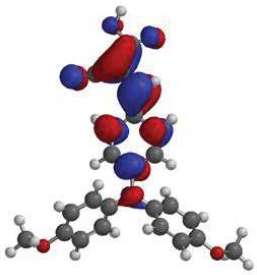

1 LUMO

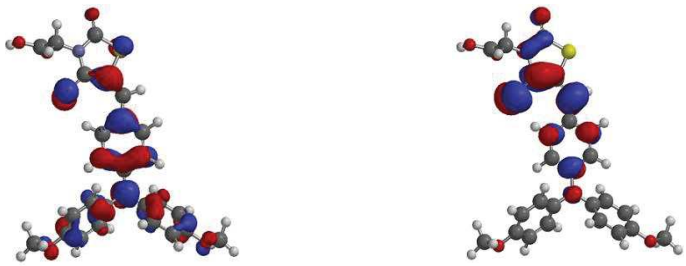

2 HOMO **2 LUMO**

Figure 4. Molecular orbital distributions of **1** and **2**.

For both **1** and **2**, HOMOs are distributed over the whole molecular structures. LUMO of **1** and **2** are mainly concentrated on cyanoacrylic acid and rhodanine moieties, especially on carbonyl and thiocarbonyl groups, as well as on the neighbouring benzene rings. The energies of HOMO and LUMO for **1** were found to be -5.15 and -2.12 eV, respectively, and those estimated for **2** were -5.02 and -2.48 eV, respectively. It was found that the calculated values are in good agreement with the experimental CV data.

Ionization potential values of thin solid layers (IP_{PE}) of derivatives **1**, **2** were estimated by photoelectron emission spectrometry. Photoelectron emission spectra of the solid layers of **1, 2** are depicted in Fig. 5. The IP_{PE} values of the solid samples of **1** and **2** were found to be comparable (5.26 and 5.29 eV, respectively).

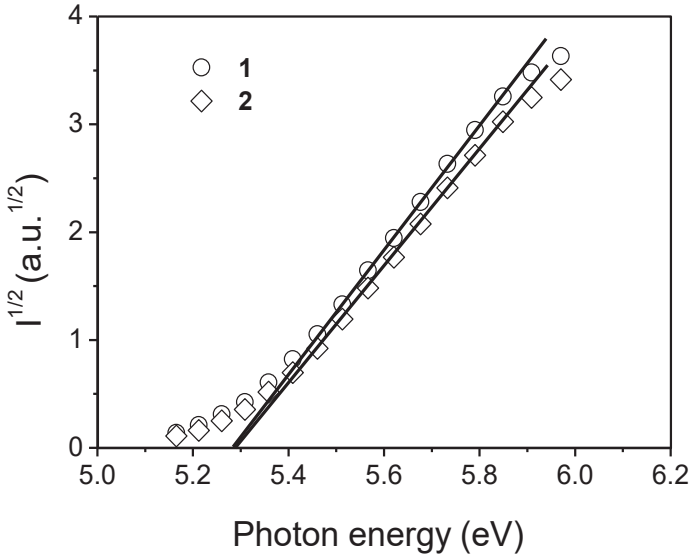

Figure 5. Photoelectron emission spectra of the solid films of **1** and **2**.

Charge-transporting properties of the layers of compound **1** were studied by time-of-flight (TOF) technique. To prepare the sample with the structure of ITO/organic layer/Al, the layer of compound **1** the sample was deposited by thermovacuum method. It was not possible to prepare the sample of compound **2** for the TOF measurements by the same method, apparently due to its relatively low thermal stability (Table 1). Hole drift mobility of 3.4×10^{-6} cm^2/Vs at electric field of 5.2×10^5 V/cm was obtained for compound **1**. Hole mobilities of the layer of **1** were found to be strongly dependent upon electric field. This dependence could be well described by a Poole-Frenkel type mobility using formula $\mu=\mu_0 e^{\alpha\sqrt{E}}$ [26]. Zero-field mobilities (μ_0) and field dependence parameter (α) are given in Fig. 6. Relatively high dependence of hole mobilities versus electric field for derivative **1** can apparently be explained by the dispersive hole transport which is betrayed by TOF transients shown in the insert of Fig. 6.

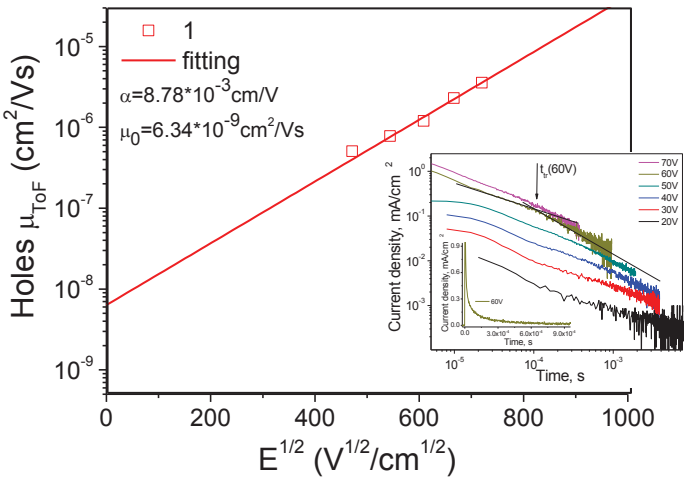

Figure 6. Electric field dependence of hole drift mobility for the layer of derivative **1**. Insert shows TOF transients for hole transport and one of the transient curves in the linear plot.

NLO properties

Kerr and two-photon absorption effects describe materials refractive index and absorption changes, respectively, due to optical irradiance:

$$n=n_0+n_2I, \quad (1)$$

$$\alpha=\alpha_0+\alpha_2I, \quad (2)$$

where n_0 is linear refractive index, α_0 - linear absorption coefficient, n_2 - Kerr coefficient, α_2 is TPA coefficient and I is optical intensity.

We studied Kerr and two-photon absorption effects of selected molecules to better understand how different acceptor groups influence third-order NLO properties. Organic molecules were dissolved in chloroform and contained in 2 mm thick optical quartz cells.

To study Kerr and two-photon absorption effects we implemented the Z-scan method. Details regarding experimental setup can be found in reference [27]. Laser beam was focused using lens with 11 cm focal length. Light transmitted through sample was measured simultaneously with open-aperture detector and closed-aperture detector with 1 mm aperture separating less than 1 % of incident light. Laser beam waist radius at focus was calculated to be w_0=26 μm. This allowed to employ thin-sample approximation for data fitting [27]. To acquire Kerr and two-photon absorption coefficients from experimental data we employed analytical expressions derived using Gaussian decomposition method [28]. During Z-scan experiment we measured how materials transmittance changes due to optical irradiance. For Kerr effect transmittance can be expressed as:

$$T(z)=1+\frac{4\Delta\Phi\frac{z}{z_0}}{\left(\frac{z^2}{{z_0}^2}+1\right)\left(\frac{z^2}{{z_0}^2}+9\right)}, \qquad (3)$$

where z - sample position, z_0 - Rayleigh length and $\Delta\Phi$ is phase change defined as:

$$\Delta\Phi=kn_2L_{eff}I, \qquad (4)$$

where k - wave number and L_{eff} - effective sample length defined as:

$$L_{eff}=\frac{1-e^{-\alpha L}}{\alpha}, \qquad (5)$$

In case of TPA, transmittance of measured medium can be expressed as:

$$T(z)=\sum_{m=0}^{\infty}\frac{\left(-\frac{q}{\left(1+\frac{z^2}{{z_0}^2}\right)}\right)^m}{(m+1)^{3/2}}, \qquad (6)$$

where q is TPA amplitude defined as:

$$q=\alpha_2L_{eff}I, \qquad (7)$$

While TPA coefficient allows us to compare different NLO sample, it does not allow us to compare molecules. For this we calculated two-photon absorption cross-section values that characterize single

molecule contribution to two-photon absorption effect. Two-photon absorption cross-section can be calculated using the following equation [29]:

$$\sigma_{TPA}=\frac{h\nu}{N}\alpha_2, \qquad (8)$$

where hν is photon energy and N molecule concentration per cm^3. To use analytical equations (3) and (6) NLO medium needs to fit weak nonlinear model for which two conditions need to be satisfied - phase change $|\Delta\Phi|<\pi$ and two-photon absorption amplitude $|q|<1$ [28].

Example for compound **1** experimental data is shown in Fig. 7. Phase changes for different concentration samples in case of **1** are shown in Fig. 8. It is evident that by increasing compound **1** concentration the phase changes decrease. This leads to conclusion that compound **1** possess negative Kerr coefficient. Acquired values for NLO coefficients for all molecules are listed in Table 4.

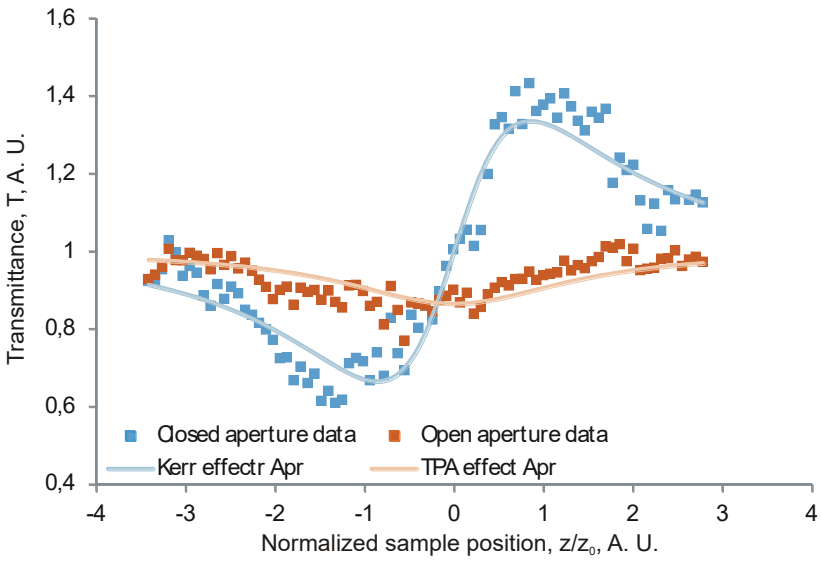

Figure 7. Z-scan experimental data for **1** fitted with corresponding analytical approximations (Apr).

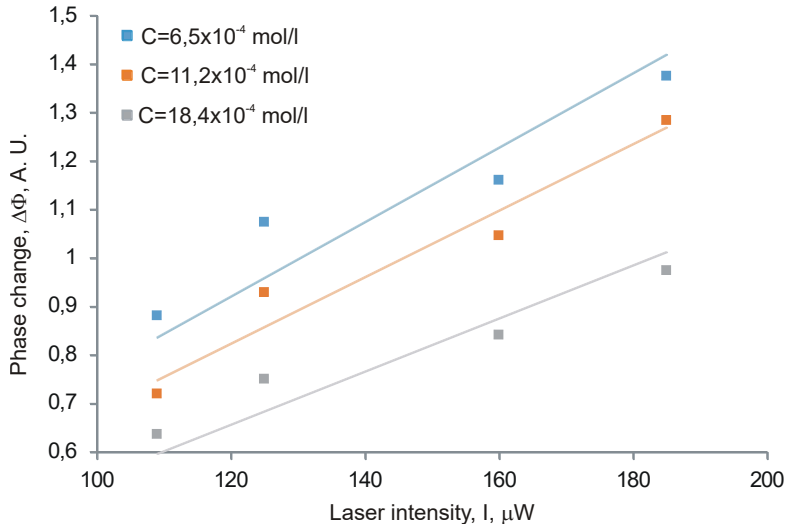

Figure 8. Phase change ΔΦ as function of laser intensity.

Table 4. Kerr, TPA and two-photon absorption cross-section values of studied molecules.

Compound	M, g/mol	n_2, $cm^2/W*10^{-12}$	α_2, $cm/W*10^{-8}$	σ_{TPA}, GM
I	305.37	0.106±0.023	-	-
II	333.38	0.249±0.035	-	-
1	400.427	-1.875±0.22	7.10±0.86	592±72
2	506.593	-1.93±0.20	-	-

Real and imaginary parts of third-order susceptibility can be defined as [30]:

$$\chi_{Re}^{(3)} = \left(4 \cdot \frac{\varepsilon_0 \cdot c \cdot n_0^2}{3}\right) \cdot n_2 \left(\frac{m^2}{W}\right), \quad (9)$$

$$\chi_{Im}^{(3)} = \left(\frac{\varepsilon_0 \cdot c \cdot n_0^2 \cdot \lambda}{3 \cdot \pi}\right) \cdot \alpha_2 \left(\frac{m}{W}\right), \quad (10)$$

where λ - laser wavelength, ε_0 - vacuum dielectric constant, n_0 - refractive index an c - speed of light. Additionally, we carried out quantum chemical calculations of second-order hyperpolarizability real

part γ_A using CPKS method in Gaussian 9. Further information about calculation parameters can be found in [27]. Experimental values for second-order hyperpolarizability were calculated using equation (11) and presented alongside third-order susceptibility values in Table 5 [31].

$$\gamma_E = \frac{\chi^{(3)}_{Re}}{\left[\frac{1}{3}(n_0^2+2)\right]^4 \cdot N}, \qquad (11)$$

Table 5. Real and imaginary part of third order susceptibility and absolute experimental and quantum calculation values of second-order hyperpolarizability. For the comparison, the second-order hyperpolarizability values of triphenylamine are given.

Compound	χ_{Re}, $m^2/V^2 \cdot 10^{-19}$	χ_{Im}, $m^2/V^2 \cdot 10^{-19}$	γ_A, esu $\cdot 10^{-34}$	$\lvert\gamma_E\rvert$, esu $\cdot 10^{-34}$
Triphenylamine				
[27]			0.58	1.69±0.57
I	1.085±0.24	-	1.09445	3.74±0.81
II	2.55±0.35	-	2.0351	9.6±1.4
1	-19.2±2.2	6.23±0.76	5.47653	87±10
2	-19.8±2.1	-	10.84	113±12

From all of the molecules only compound **1** possesses two-photon absorption coefficient due to considerable absorption at 532 nm. By comparing the values of Kerr coefficient it is evident that by adding a stronger acceptor group we increase the magnitude of Kerr effect. Experimental and quantum calculation values for second-order hyperpolarizability are shown in Fig. 9.

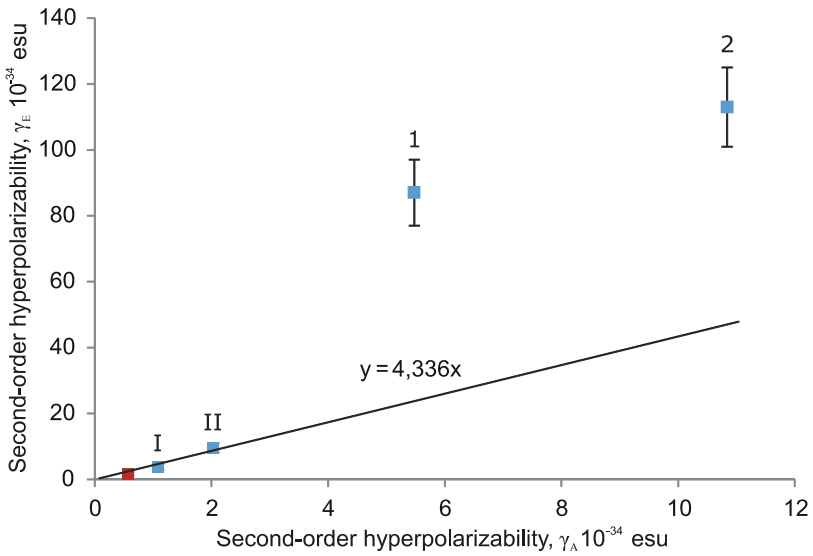

Figure 9. Experimental and quantum calculation values of second-order hyperpolarizability. Blue point indicate molecules studied in this paper while red dot indicates triphenylamine studied in our previous paper [32].

It is evident that derivatives **I** and **II** gives a similar slope values as other derivatives of triphenylamine reported in other papers [27,32]. At the same time, derivatives **1** and **2** displays much larger difference between experimental and quantum calculation values. We speculate that this is due to aggregation processes that can lead to larger third-order NLO values. Similar enhancement of NLO properties due to aggregation has been previously reported in literature [33].

Photovoltaic properties

The photovoltaic properties of compounds **1** and **2**, used as dyes, were investigated by fabricating solid-state dye sensitized solar cells with spiro-OMeTAD as p-type organic hole transporting material (HTM). The device structure was FTO/TiO_2/Dye/Spiro-OMeTAD/Ag.

Knowing the IP values of 5.23 and 5.18 eV and the EA values of 2.91 and 2.70 eV, respectively for **1** and **2**, we can expect that these dyes would be suitable i) for electron transfer to the TiO_2 nanostructured electrode as well as ii) to be regenerated by HTM. In comparison, IP and EA values of **D102** are 5.32 and 3.38 eV respectively [34]. EA values of the new dyes are expected to prevent any electron transfer from the dye to the LUMO of the spiro-OMeTAD (EA value of the HTM is 2.05 eV) [35]. In summary, the energy levels of the synthesized dyes are clearly well suited for FTO/TiO_2/Dye/Spiro-OMeTAD/Ag device.

Usually, the solvent used to prepare the solution of **D102** is a mixture of acetonitrile and *tert*-butanol (ACN/*tert*-BuOH). The solution of dye **1** has been prepared and deposited under these conditions. Nevertheless, dye **2** was found to be hardly soluble in this solvent mixture. That is why THF as solvent was preferred for dye **2**. The same dye concentration (0.06 mM) was chosen for both compounds **1** and **2**.

Table 6. Photovoltaic characteristics of the devices FTO/TiO_2/Dye/Spiro-OMeTAD/Ag with dye **1** (in ACN/*tert*-butanol) and **2** (in THF).

Parameters	**1**	**2**
V_{OC} (V)	0.65	0.68
Jsc ($mAcm^{-2}$)	3.39	4.08
FF	0.46	0.66
PCE (%)	1.02	2.09

Fig. 10a shows photocurrent-voltage curves and IPCE spectra of **1-** and **2**-sensitized DSSCs. Photovoltaic parameters are summarized in Table 6. Photocurrent of the **2**-sensitized DSSC is

higher than that of the **1**-sensitized one, which is due to more delocalized electron distribution in the HOMO state (see Fig. 4). The open-circuit voltage (V_{OC}) are of ca. 0.65 V for both dyes. The higher V_{OC} (0.80 V) observed for the organic **D102** dye (Table S1) is probably related to the recombination kinetics at the TiO_2/Dye/HTM interface. Indeed, the energy offset for electron injection from the LUMO level of the dye to the TiO_2 conduction band is found to be much larger for compounds **1** and **2** compared to **D102**, which can explain a substantial energy loss of the photo-excited electrons. Moreover, the energy difference between the LUMO of compound **2** (and in less extend of compound **1**) and LUMO level of spiro-OMeTAD is largely reduced compared to **D102** (Fig. S3). The energy barrier for direct electron injection to spiro-OMeTAD is therefore reduced, which can favor charge recombination and prevent efficient charge injection. Such phenomenon is in agreement with the larger dark current observed under reverse applied voltage (see Fig. S4). Finally, although the power conversion efficiency of the devices with dye **1** is quite low (1.02%), the devices built with dye **2** show interesting PCE (2.09%), close to that **D102** reference (2.47%). The limited PCE for the devices built with dye **1** is most likely due to the blue-shift in optical absorption, which is less favorable for efficient charge generation. Since the maximum of absorption of **1** is shifted to lower wavelengths compared to those of **D102** and **2**, we can observe the beginning of a screen effect (overlapping of both dye and HTM absorption). Although several devices have been prepared (Fig. S5) and even if the PCE are lower than that of the **D102** reference dye without further optimizations (i.e. in concentration), the results show a promising tendency for both dyes.

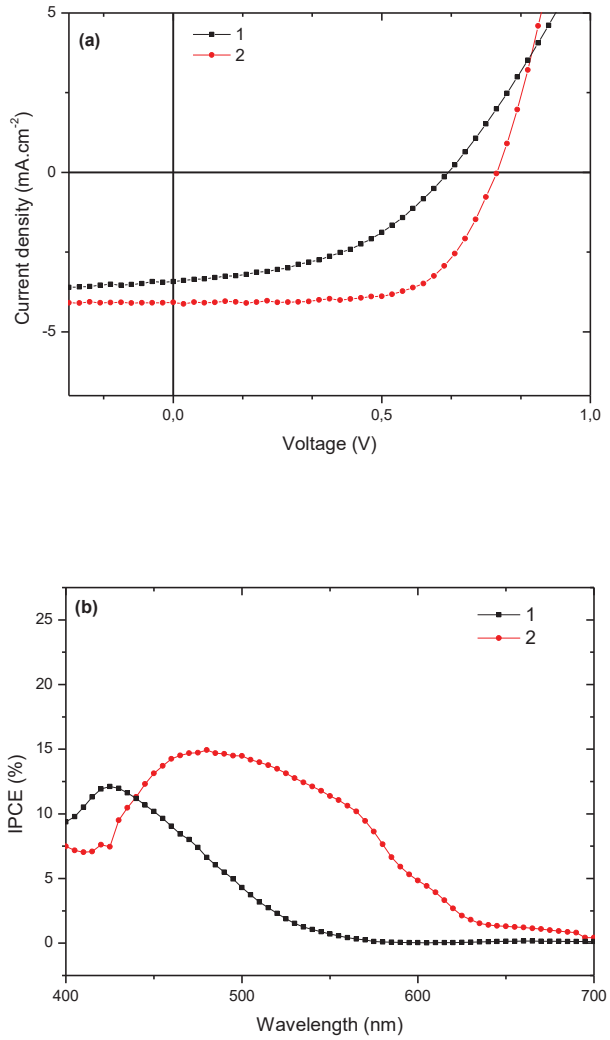

Figure 10. (a) Photocurrent density-voltage curves under illumination and (b) incident photon-to-current conversion efficiency (IPCE) spectra of **1**- and **2**-sensitized DSSCs.

Fig. 10b shows the external quantum efficiency (EQE) spectra of the solid-state DSSC [FTO/TiO_2/Dye/Spiro-OMeTAD/Ag] containing **1** and **2,** recorded under the monochromatic illumination. The devices based on **2** show a broad response which extends up to 650 nm, while compound **1** only exploits incoming photons up to 520 nm. The IPCE spectra are in

agreement with the optical absorption data, where the maximum absorption of dye **1** is blue-shifted leading to an increased screening effect of the solar light. IPCE shows clearly that dye **2** is better suited in terms of absorption for solid-state DSSC.

Conclusions

Dimethoxy-substituted triphenylamine derivatives containing cyanoacrylic acid and rhodanine-3-acetic acid moieties were synthesized by Knoevenagel condensation. The target derivatives form molecular glasses with glass transition temperatures of 83 and 61 ºC. They show moderate thermal stability with the temperatures of degradation onsets of 283 and 195 ºC. The cyclic voltammetry measurements revealed close ionization potential (5.23 and 5.18 eV) and electron affinity values (-2.91 and -2.70 eV) in the solid state. The layer of derivative conatining cyanoacrylic acid moiety showed time-of-flight hole drift mobility of 3.4×10^{-6} cm^2/Vs at electric field of 5.2×10^5 V/cm. This compound also showed two-photon absorption effect as it was the only compound exhibiting considerable absorption at 532 nm. Compounds containing acceptor groups possessed larger nonlinear refractive index values than dimethoxy substituted triphenylamines. Dye sensitized solar cells with the structure FTO/TiO_2/Dye/Spiro-OMeTAD/Ag were fabricated using the synthesized compounds as dyes. The photovoltaic properties of the devices were found to be in agreement with the electronic and optical properties. The dye containing a rhodanine-3-acetic acid moiety exhibited a promising power conversion efficiency of 2.09% in solid state dye sensitized solar cell using the spiro-OMeTAD as hole transporting compound.

Compliance with ethical standards

Conflict of interest. The authors declare that they have no conflict of interest.

Acknowledgements

This research was funded by the Région Centre, the Tunisian ministry of research, University of Monastir and the French ministry of Higher Education and Research. J. Bouclé would like to thank the Sigma-Lim LabEx environment for financial supports, and the PLATINOM facility at XLIM laboratory regarding device fabrication and characterizations. This research was funded by a grant (No. S-LZ-19-2) from the Research Council of Lithuania.

References

[1] a) Jung JW, Jo JW, Jung EH, Jo WH (2016) Recent progress in high efficiency polymer solar cells by rational design and energy level tuning of low bandgap copolymers with various electron-withdrawing units, Org Electron 31:149–70; b) Kahle FJ, Saller C, Köhler A, Strohriegl P (2017) Crosslinked semiconductor polymers for photovoltaic applications, Adv Energy Mater 7:1700306-1700315; c) Lincker F, Delbosc N, Bailly S et al (2008) Fluorenone-based molecules for bulk-heterojunction solar cells: Synthesis, characterization, and photovoltaic properties, Adv Funct Mater 18:3444–53.

[2] a) Grätzel M, O'Regan B (1991) A low-cost, high-efficiency solar cell based on dye-sensitized colloidal TiO2 films, Nature 353:737–40; b) Ning Z, Fu Y, Tian H (2010) Improvement of dye-sensitized solar cells: What we know and what we need to know, Energ Environ Sci 3:1170–81; c)

Ning Z, Tian H (2009) Triarylamine: A promising core unit for efficient photovoltaic materials, Chem Commun 5483–95.

[3] a) Hagfeldt A, Cappel UB, Boschloo G et al (2010) Dye-sensitized solar cells, Chem Rev 110:6595–663; b) Tian HN, Sun LC (2011) Iodine-free redox couples for dye-sensitized solar cells, J Mater Chem 21:10592–10601; c) Wang M, Grätzel C, Zakeeruddin SM, Grätzel M (2012) Recent developments in redox electrolytes for dye-sensitized solar cells, Energ Environ Sci 5:9394–405.

[4] a) Yella A, Lee H, Tsao HN et al (2011) Porphyrin-sensitized solar cells with cobalt (II/III)-based redox electrolyte exceed 12 percent efficiency, Science 334:629–33; b) Mathew S, Yella A, Gao P et al (2014) Dye-sensitized solar cells with 13% efficiency achieved through the molecular engineering of porphyrin sensitizers, Nat Chem 6:242–7.

[5] Cells SDS, Leijtens T, Ding I et al (2012) Hole transport materials with low glass transition temperatures and high solubility for application in solid state DSC, ACS Nano 1455–62.

[6] Lygaitis R, Schmaltz B, Degutyte R et al (2014) Star-shaped triphenylamine-based molecular glass for solid state dye sensitized solar cell applicationm Synth Met 195:328–34.

[7] Burschka J, Dualeh A, Kessler F et al (2011) Tris(2-(1 H-pyrazol-1-yl)pyridine)cobalt(III) as p-type dopant for organic semiconductors and its application in highly efficient solid-state dye-sensitized solar cells, J Am Chem Soc 133:18042–5.

[8] Melhem H, Simon P, Beouch L et al (2011) TiO2 nanocrystals synthesized by laser pyrolysis for the up-scaling of efficient solid-state dye-sensitized solar cells, Adv Energy Mater 1:908–16.

[9] Xu B, Bi D, Hua Y et al (2016) A low-cost spiro[fluorene-9,9′-xanthene]-based hole transport material for highly efficient solid-state dye-sensitized solar cells and perovskite solar cells, Energ Environ Sci 9:873–877.

[10] Zeng W, Cao Y, Bai Y et al (2010) Efficient dye-sensitized solar cells with an organic photosensitizer featuring orderly conjugated ethylenedioxythiophene and dithienosilole blocks, Chem Mater 22:1915–25.

[11] a) Mahmood A (2016). Triphenylamine based dyes for dye sensitized solar cells: A review, Sol Energy 123:127–44; b) Yum JH, Hagberg DP, Moon SJ et al (2009) A light-resistant organic sensitizer for solar-cell applications, Angew Chem - Int Ed 48:1576–80.

[12] Wang C, Li J, Cai S et al (2012) Performance improvement of dye-sensitizing solar cell by semi-rigid triarylamine-based donors, Dyes Pigm 94:40–8.

[13] Zhang L, Liu Y, Wang Z, Liang M, Sun Z, Xue S (2010) Synthesis of sensitizers containing donor cascade of triarylamine and dimethylarylamine moieties for dye-sensitized solar cells, Tetrahedron 66:3318–25.

[14] a) Abbotto A, Manfredi N, Marinzi C et al (2009) Di-branched di-anchoring organic dyes for dye-sensitized solar cells, Energ Environ Sci 2:1094–101; b) Jiang X, Karlsson KM, Gabrielsson E et al (2011) Highly efficient solid-state dye-sensitized solar cells based on triphenylamine dyes, Adv Funct Mater 21:2944–52.

[15] Hu D, Hu Y, Huang W, Zhang Q (2012) Two-photon induced data storage in hydrogen bonded supramolecular azopolymers, Opt Commun 285:4941–5.

[16] Ahadi S, Granpayeh N (2015) Femtosecond all-optical switching based on asymmetric plasmonic Kerr Fabry-Perot resonators, Opt Commun 349:36–41.

[17] Belfield KD, Morales AR, Kang BS et al (2004) Synthesis, characterization, and optical properties of new two-photon-absorbing fluorene derivatives, Chem Mater 16:4634–41.

[18] Webster S, Fu J, Padilha LA et al (2008) Comparison of nonlinear absorption in three similar dyes: Polymethine, squaraine and tetraone, Chem Phys 348:143–51.

[19] Padilha LA, Webster S, Przhonska OV et al (2009) Nonlinear absorption in a series of donor-π-acceptor cyanines with different conjugation lengths, J Mater Chem 19:7503–13.

[20] Xu W, Peng B, Chen J, Liang M, Cai F (2008) New triphenylamine-based dyes for dye-sensitized solar cells, J Phys Chem C 112:874–80.

[21] Roquet S, Cravino A, Leriche P, Alévêque O, Frère P, Roncali J (2006) Triphenylamine-thienylenevinylene hybrid systems with internal charge transfer as donor materials for heterojunction solar cells, J Am Chem Soc 128:3459–66

[22] Lai RY, Fabrizio EF, Lu L, Jenekhe SA, Bard AJ (2001) Synthesis, cyclic voltammetric studies, and electrogenerated chemiluminescence of a new donor - Acceptor molecule: 3,7-[bis[4-phenyl-2-quinolyl]]-10-methylphenothiazine, J Am Chem Soc 123:9112–9118.

[23] Can M, Yigit MZ, Seintis K et al (2014) Synthesis of two tri-arylamine derivatives as sensitizers in dye-sensitized solar cells: Electron injection studies and photovoltaic characterization, Synth Met 188:77–85.

[24] Drake KF, Van Duyne RP, Bond AM (1978) Cyclic differential pulse voltammetry: A versatile instrumental approach using a computerized system, J Electroanal Chem 89:231–46.

[25] Spartan'14 for Windows Version 1.1.2. 1840 Von Karman Avenue, Suite 370, Irvine, CA.

[26] Frenkel J (1938) On pre-breakdown phenomena in insulators and electronic semi-conductors [3], Phys Rev 54:647–8.

[27] Bundulis A, Nitiss E, Mihailovs I, Busenbergs J, Rutkis M (2016) Study of structure-third-order susceptibility relation of indandione derivatives, J Phys Chem C 120:27515–22.

[28] Sheik-Bahae M, Said AA, Wei TH, Hagan DJ, Van Stryland EW (1990) Sensitive measurement of optical nonlinearities using a single beam, IEEE J Quantum Electron 26:760–9.

[29] Ajami A, Gruber P, Tromayer M et al (2015) Evidence of concentration dependence of the two-photon absorption cross section: Determining the “true” cross section value, Opt Mater (Amst) 47:524–9.

[30] del Coso R, Solis J (2004) Relation between nonlinear refractive index and third-order susceptibility in absorbing media. J Opt Soc Am B 21:640.

[31] Sharafudeen KN, Adithya A, Vijayakumar S, Sudheesh P, Kalluraya B, Chandrasekharan K (2011) Multiphoton absorption process and self-focusing effect in coumarin derivative doped PMMA films by Z-scan and optical limiting studines, Curr Appl Phys 11:1089–93.

[32] Gudeika D, Bundulis A, Mihailovs I, Volyniuk D, Rutkis M, Grazulevicius JV (2017) Donor and acceptor substituted triphenylamines exhibiting bipolar charge-transporting and NLO properties, Dyes Pigm 140:431–40.

[33] Yang L, Chen Z, Zhang S et al (2014) The tunable third-order optical nonlinearities of a diarylethene-zinc phthalocyanine hybrid, Dyes Pigm 102:251–6.

[34] Wang H, Liu G, Li X et al (2011) Highly efficient poly(3-hexylthiophene) based monolithic dye-sensitized solar cells with carbon counter electrode, Energ Environ Sci 4:2025–9.

[35] Teh CH, Daik R, Lim EL et al (2016) A review of organic small molecule-based hole-transporting materials for meso-structured organic-inorganic perovskite solar cells, J Mater Chem A 4:15788–822.

LIST

Table 1. Thermal characteristics of derivatives **1** and **2**.

Table 2. UV and emission data of dilute solutions (10^{-5} M) of **1** and **2** in toluene.

Table 3. Electrochemical characteristics of compounds **1** and **2**.

Table 4. Kerr, TPA and TPA cross-section values of studied molecules.

Table 5. Real and imaginary part of third order susceptibility and absolute experimental and quantum calculation values of second-order hyperpolarizability. For the comparison, the second-order hyperpolarizability values of triphenylamine are given.

Table 6. Photovoltaic characteristics of the devices FTO/TiO_2/Dye/Spiro-OMeTAD/Ag with dye **1** (in ACN/*tert*-butanol) and **2** (in THF).

Figure 1. DSC thermograms of **1**.

Figure 2. Normalized UV and FL spectra of dilute solutions of **1** and **2** in toluene at 298 K.

Figure 3. (a) CV of **1** recorded in an inert atmosphere (100 mV/s vs Ag/Ag^+); (b) DPV curves of 1×10^{-6} M of compounds **1** and **2** in 0.1M Bu_4NBF_6/DCM electrolyte.

Figure 4. Molecular orbital distributions of **1** and **2**.

Figure 5. Photoelectron emission spectra of the solid films of **1** and **2**.

Figure 6. Electric field dependence of hole drift mobility for the layer of derivative **1**. Insert shows TOF transients for hole transport and one of the transient curves in the linear plot.

Figure 7. Z-scan experimental data for **1** fitted with corresponding analytical approximations (Apr).

Figure 8. Phase change $\Delta\Phi$ as function of laser intensity.

Figure 9. Experimental and quantum calculation values of second-order hyperpolarizability. Blue point indicate molecules studied in this paper while red dot indicates triphenylamine studied in our previous paper [35].

Figure 10. (a) Photocurrent density-voltage curves under illumination and (b) incident photon-to-current conversion efficiency (IPCE) spectra of **1**- and **2**-sensitized DSSCs.

LIST OF TABLES

Table 1. Thermal characteristics of derivatives **1** and **2**.

Derivative	T_m, [°C]	T_g, [°C] (2nd heating)	$T_{ID-5\%}$, [°C]
1	201	83	283
2	121	61	195

T_g - glass transition point, T_m - melting point (10 °C/min, nitrogen atmosphere). $T_{ID-5\%}$ is 5% (20 °C/min under nitrogen).

Table 2. UV and emission data of dilute solutions (10^{-5} M) of **1** and **2** in toluene.

Compound	λ_{max}[a], nm	ε[b] (10^4 $M^{-1}cm^{-1}$)	λ_{max}[c], nm	Φ_F[d], %	Stokes shift, nm	E_g^{op} /eV[e]
1	424	2.4	552	19.56	128	2.28
2	466	1.8	553	14.25	87	2.52

[a] Wavelength of absorption maximum. [b] ε is the extinction coefficient at λ_{max} of absorption. [c] Wavelength of photoluminescence emission maximum. [d] Fluorescence quantum yield. [e] $E_g^{op} = 1240/\lambda_{edge}$, where λ_{edge} is the wavelength of absorption edge in long wave direction.

Table 3. Electrochemical characteristics of derivatives **1** and **2**.

Derivative	E^{ox}_{onset} vs Fc /V[a]	IP_{CV} /eV[b]	EA_{CV} /eV[b]	IP_{PE} /eV[c]
1	0.43	5.23	-2.91	5.26
2	0.38	5.18	-2.70	5.29

[a] E^{ox}_{onset} is oxidation potential *vs.* Fc/Fc^{+}; [b] Ionization potential, electron affinity values estimated according to the equation $IP_{CV} = -(E^{ox}_{onset}+4.8)$; (where E^{ox}_{onset} is onset oxidation potential *vs.* the Fc^{+}/Fc); $EA_{CV} = -(|IP_{CV}|-E^{opt}_{g})$; [c] The values of ionization potentials (IP_{PE}).

Table 4. Kerr, TPA and TPA cross-section values of studied molecules.

Compound	M, g/mol	n_2, $cm^2/W*10^{-12}$	α_2, $cm/W*10^{-8}$	σ_{TPA}, GM
I	305.37	0.106±0.023	-	-
II	333.38	0.249±0.035	-	-
1	400.427	-1.875±0.22	7.10±0.86	592±72
2	506.593	-1.93±0.20	-	-

Table 5. Real and imaginary part of third order susceptibility and absolute experimental and quantum calculation values of second-order hyperpolarizability. For the comparison, the second-order hyperpolarizability values of triphenylamine are given.

Compound	χ_{Re}, $m^2/V^2 \cdot 10^{-19}$	χ_{Im}, $m^2/V^2 \cdot 10^{-19}$	γ_A, esu $\cdot 10^{-34}$	$\lvert\gamma_E\rvert$, esu $\cdot 10^{-34}$
Triphenylamine				
[22]			0.58	1.69±0.57
I	1.085±0.24	-	1.09445	3.74±0.81
II	2.55±0.35	-	2.0351	9.6±1.4
1	-19.2±2.2	6.23±0.76	5.47653	87±10
2	-19.8±2.1	-	10.84	113±12

Table 6. Photovoltaic characteristics of the devices FTO/TiO_2/Dye/Spiro-OMeTAD/Ag with dye **1** (in ACN/*tert*-butanol) and **2** (in THF).

Parameters	**1**	**2**
V_{OC} (V)	0.65	0.68
Jsc ($mAcm^{-2}$)	3.39	4.08
FF	0.46	0.66
PCE (%)	1.02	2.09

LIST OF FIGURES

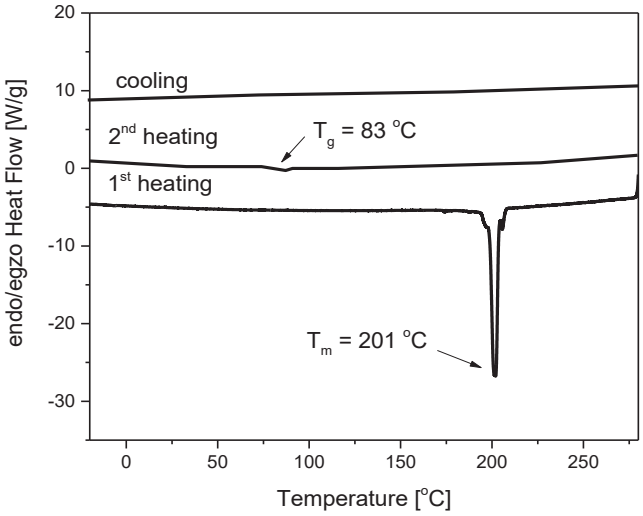

Figure 1. DSC thermograms of **1**.

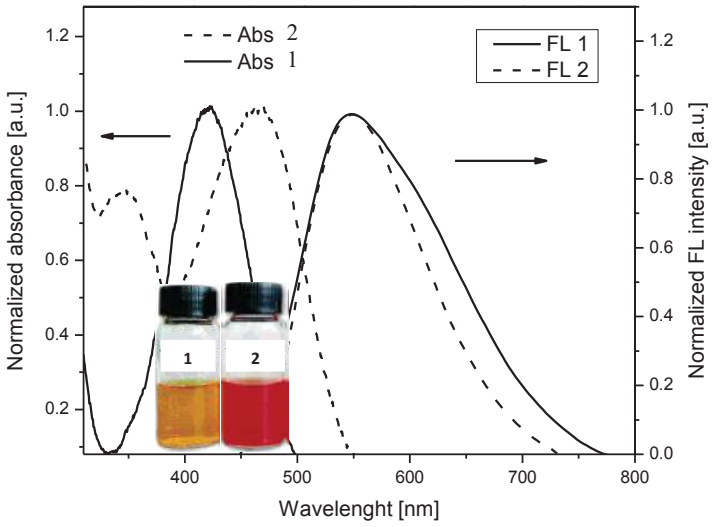

Figure 2. Normalized UV and FL spectra of dilute solutions of **1** and **2** in toluene at 298 K.

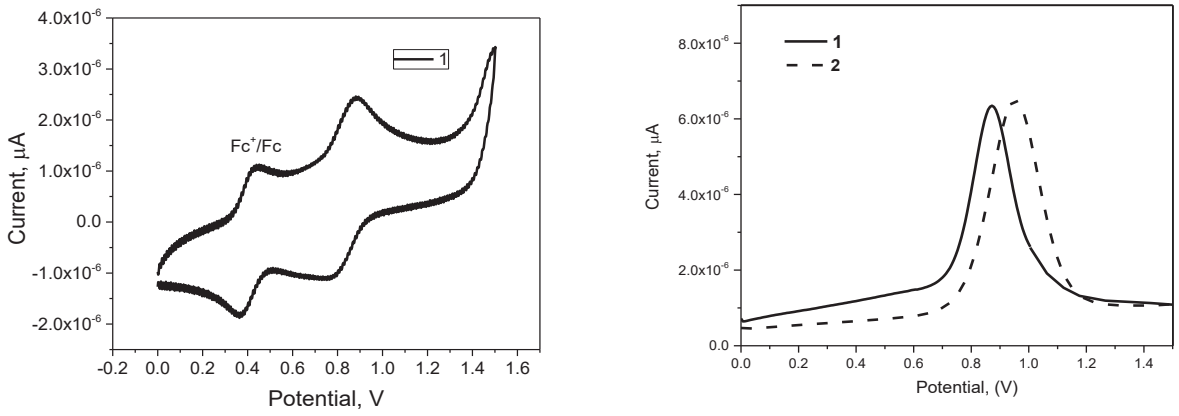

(a) (b)

Figure 3. (a) CV of **1** recorded in an inert atmosphere (100 mV/s vs Ag/Ag^{+}); (b) DPV curves of 1×10^{-6} M of compounds **1** and **2** in 0.1M Bu_4NBF_6/DCM electrolyte.

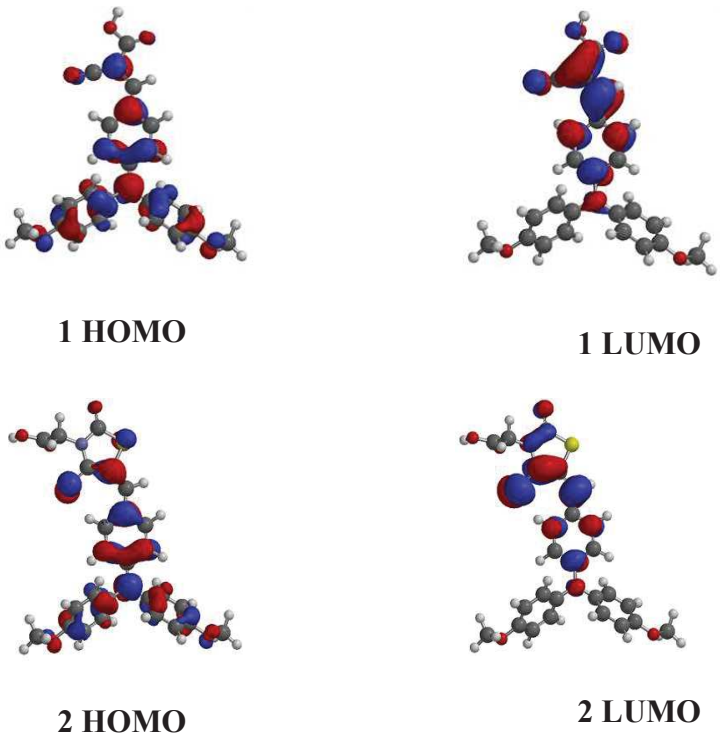

Figure 4. Molecular orbital distributions of **1** and **2**.

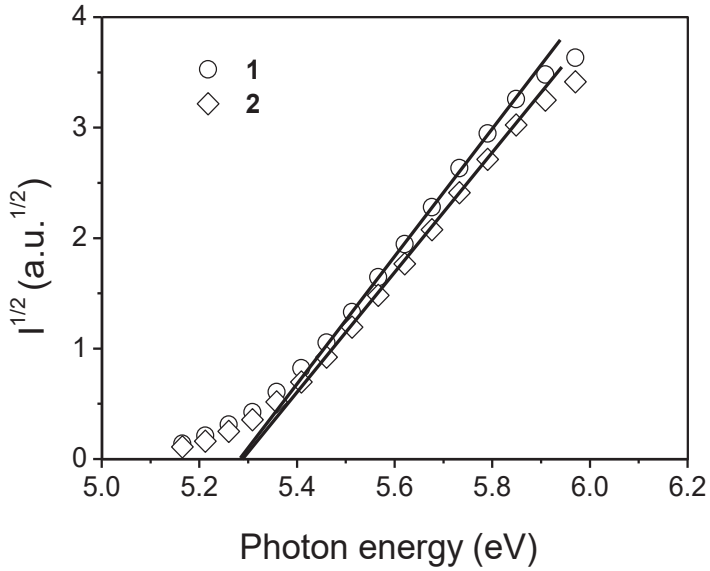

Figure 5. Photoelectron emission spectra of the solid films of **1** and **2**.

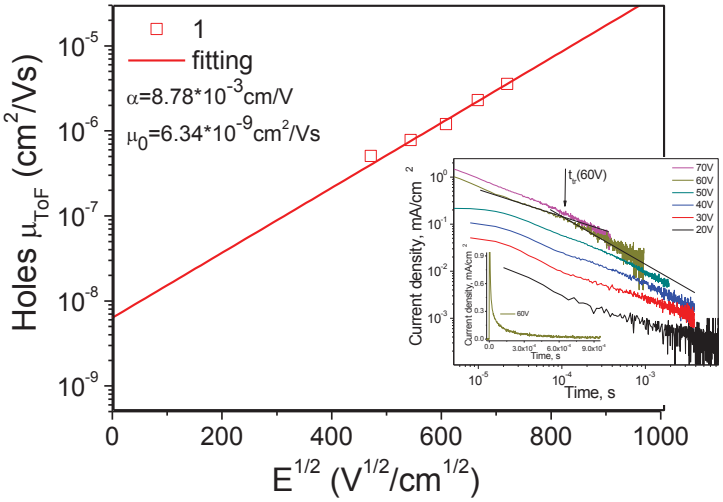

Figure 6. Electric field dependence of hole drift mobility for the layer of derivative **1**. Insert shows TOF transients for hole transport and one of the transient curves in the linear plot.

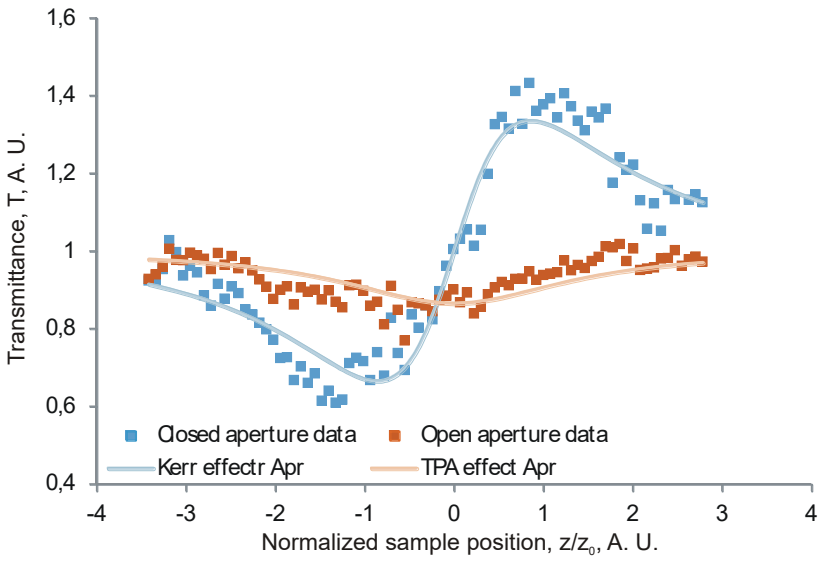

Figure 7. Z-scan experimental data for **1** fitted with corresponding analytical approximations (Apr).

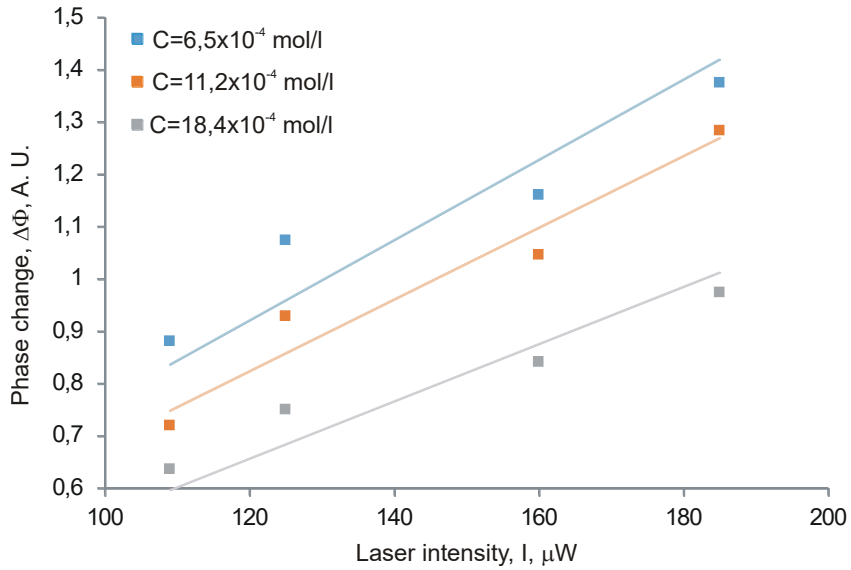

Figure 8. Phase change ΔΦ as function of laser intensity.

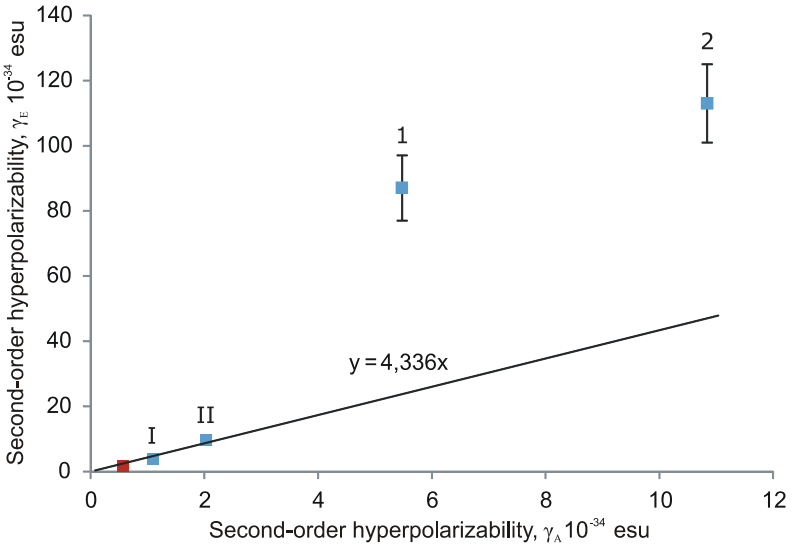

Figure 9. Experimental and quantum calculation values of second-order hyperpolarizability. Blue point indicate molecules studied in this paper while red dot indicates triphenylamine studied in our previous paper [35].

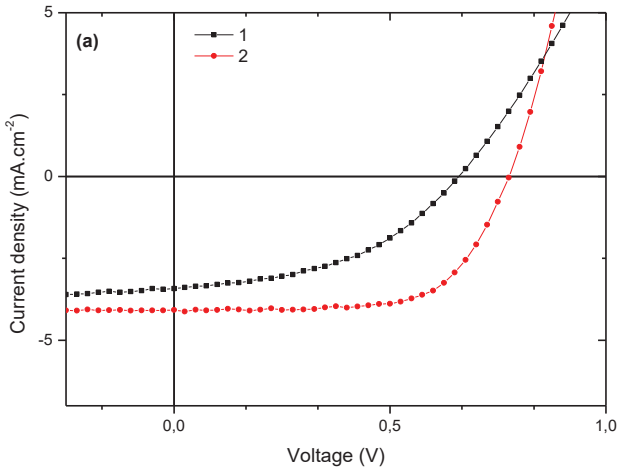

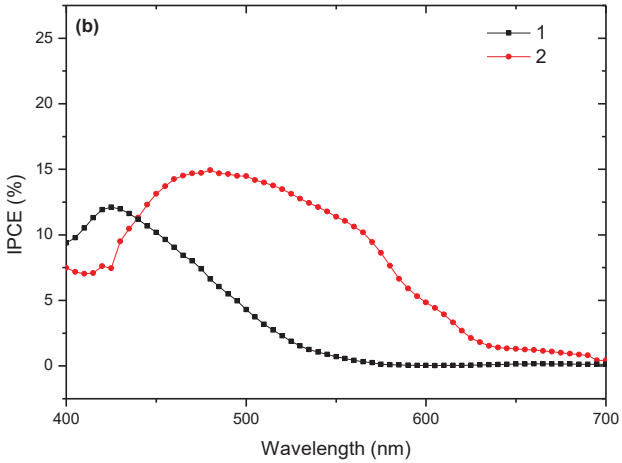

Figure 10. (a) Photocurrent density-voltage curves under illumination and (b) incident photon-to-current conversion efficiency (IPCE) spectra of **1**- and **2**-sensitized DSSCs.

Table 1. Thermal characteristics of derivatives **1** and **2**.

Derivative	T_m, [°C]	T_g, [°C] (2nd heating)	$T_{ID-5\%}$, [°C]
1	201	83	283
2	121	61	195

T_g - glass transition point, T_m - melting point (10 °C/min, nitrogen atmosphere). $T_{ID-5\%}$ is 5% (20 °C/min under nitrogen).

Table 2. UV and emission data of dilute solutions (10^{-5} M) of **1** and **2** in toluene.

Compound	λ_{max}[a], nm	ε[b] (10^4 $M^{-1}cm^{-1}$)	λ_{max}[c], nm	Φ_F[d], %	Stokes shift, nm	E_g^{op} /eV[e]
1	424	2.4	552	19.56	128	2.28
2	466	1.8	553	14.25	87	2.52

[a] Wavelength of absorption maximum. [b] ε is the extinction coefficient at λ_{max} of absorption. [c] Wavelength of photoluminescence emission maximum. [d] Fluorescence quantum yield. [e] $E_g^{op} = 1240/\lambda_{edge}$, where λ_{edge} is the wavelength of absorption edge in long wave direction.

Table 3. Electrochemical characteristics of derivatives **1** and **2**.

Derivative	E^{ox}_{onset} vs Fc /V[a]	IP_{CV} /eV[b]	EA_{CV} /eV[b]	IP_{PE} /eV[c]
1	0.43	5.23	-2.91	5.26
2	0.38	5.18	-2.70	5.29

[a] E^{ox}_{onset} is oxidation potential *vs.* Fc/Fc^+; [b] Ionization potential, electron affinity values estimated according to the equation $IP_{CV} = -(E^{ox}_{onset} + 4.8)$; (where E^{ox}_{onset} is onset oxidation potential *vs.* the Fc^+/Fc); $EA_{CV} = -(|IP_{CV}| - E^{opt}_{g})$; [c] The values of ionization potentials (IP_{PE}).

Table 4. Kerr, TPA and TPA cross-section values of studied molecules.

Compound	M, g/mol	n_2, $cm^2/W*10^{-12}$	α_2, $cm/W*10^{-8}$	σ_{TPA}, GM
I	305.37	0.106±0.023	-	-
II	333.38	0.249±0.035	-	-
1	400.427	-1.875±0.22	7.10±0.86	592±72
2	506.593	-1.93±0.20	-	-

Table 5. Real and imaginary part of third order susceptibility and absolute experimental and quantum calculation values of second-order hyperpolarizability. For the comparison, the second-order hyperpolarizability values of triphenylamine are given.

Compound	χ_{Re}, $m^2/V^2 \cdot 10^{-19}$	χ_{Im}, $m^2/V^2 \cdot 10^{-19}$	γ_A, esu $\cdot 10^{-34}$	$\lvert\gamma_E\rvert$, esu $\cdot 10^{-34}$
Triphenylamine				
[22]			0.58	1.69±0.57
I	1.085±0.24	-	1.09445	3.74±0.81
II	2.55±0.35	-	2.0351	9.6±1.4
1	-19.2±2.2	6.23±0.76	5.47653	87±10
2	-19.8±2.1	-	10.84	113±12

Table 6. Photovoltaic characteristics of the devices FTO/TiO_2/Dye/Spiro-OMeTAD/Ag with dye **1** (in ACN/*tert*-butanol) and **2** (in THF).

Parameters	**1**	**2**
V_{OC} (V)	0.65	0.68
Jsc ($mAcm^{-2}$)	3.39	4.08
FF	0.46	0.66
PCE (%)	1.02	2.09

Figure

Click here to access/download;Figure;Figure 1.jpg

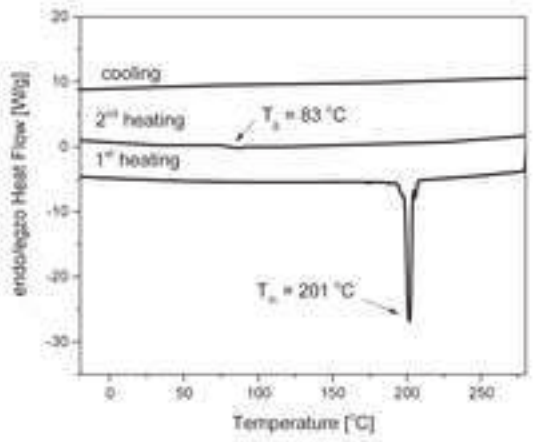

Figure 1. DSC thermograms of **1**.

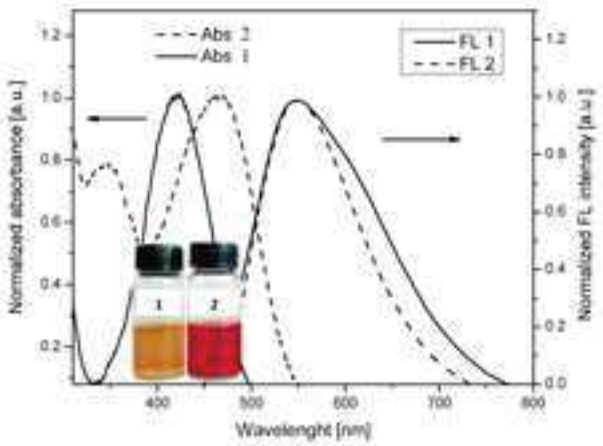

Figure 2. Normalized UV and FL spectra of dilute solutions of **1** and **2** in toluene at 298 K.

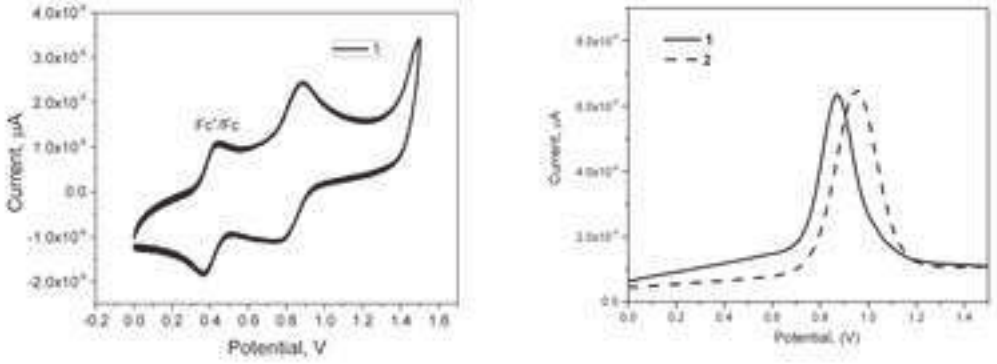

(a) (b)

Figure 3. (a) CV of **1** recorded in an inert atmosphere (100 mV/s vs Ag/Ag^+); (b) DPV curves of 1×10^{-6} M of compounds **1** and **2** in 0.1M Bu_4NBF_6/DCM electrolyte.

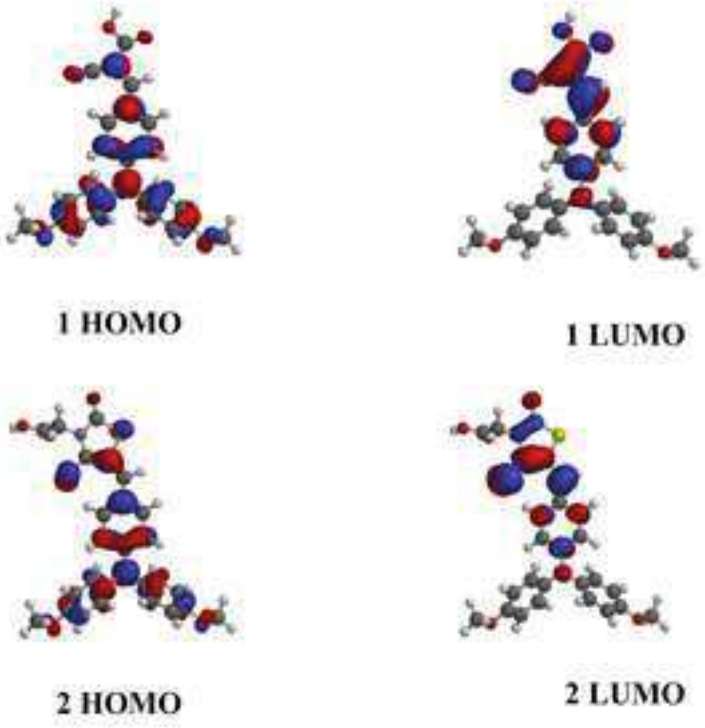

Figure 4. Molecular orbital distributions of **1** and **2**.

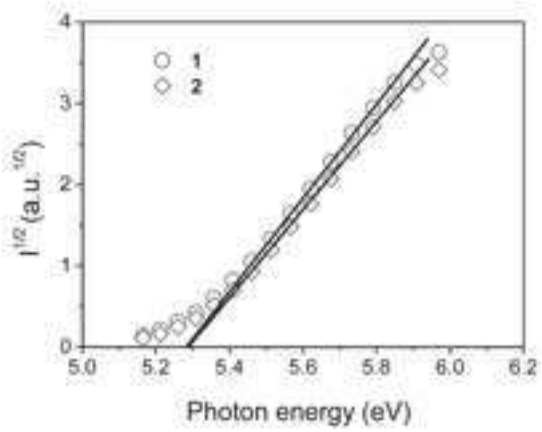

Figure 5. Photoelectron emission spectra of the solid films of **1** and **2**.

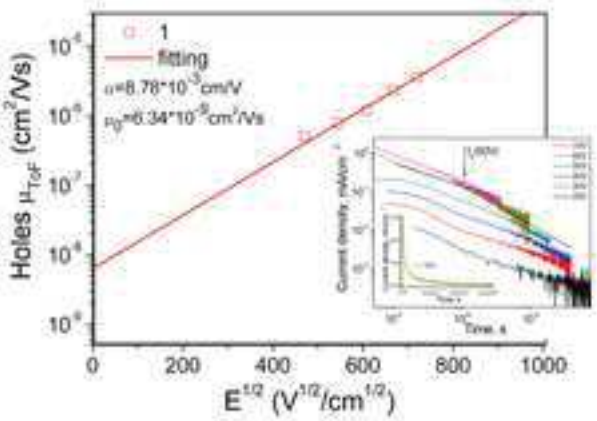

Figure 6. Electric field dependence of hole drift mobility for the layer of derivative **1**. Insert shows TOF transients for hole transport and one of the transient curves in the linear plot.

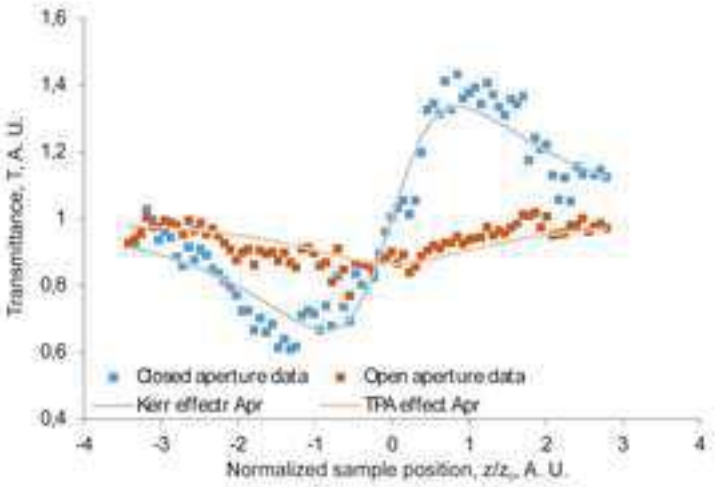

Figure 7. Z-scan experimental data for **1** fitted with corresponding analytical approximations (Apr).

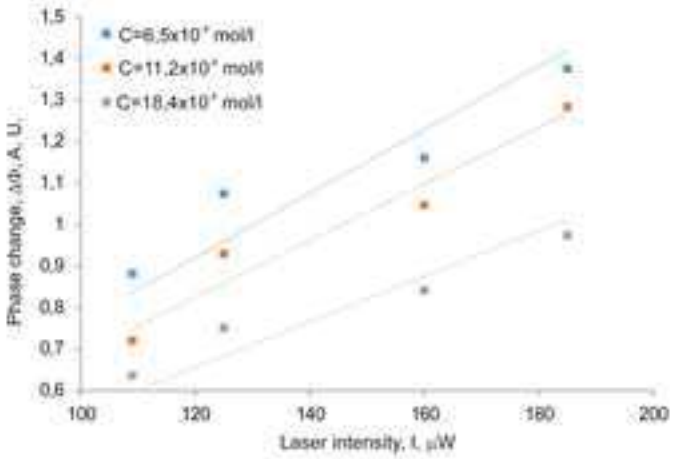

Figure 8. Phase change ΔΦ as function of laser intensity.

Figure

Click here to access/download;Figure;Figure 9.jpg

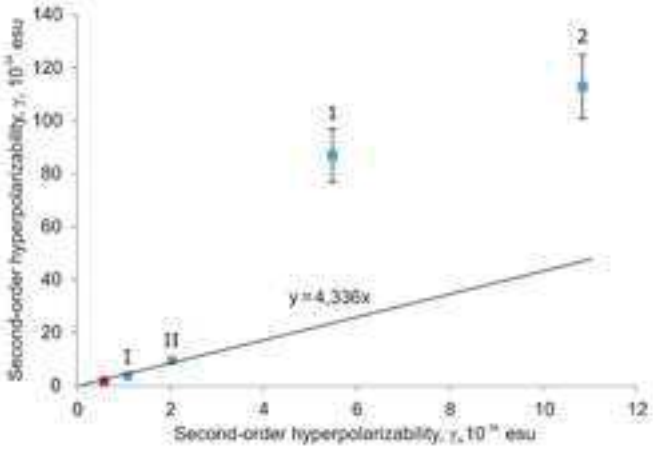

Figure 9. Experimental and quantum calculation values of second-order hyperpolarizability. Blue point indicate molecules studied in this paper while red dot indicates triphenylamine studied in our previous paper [35].

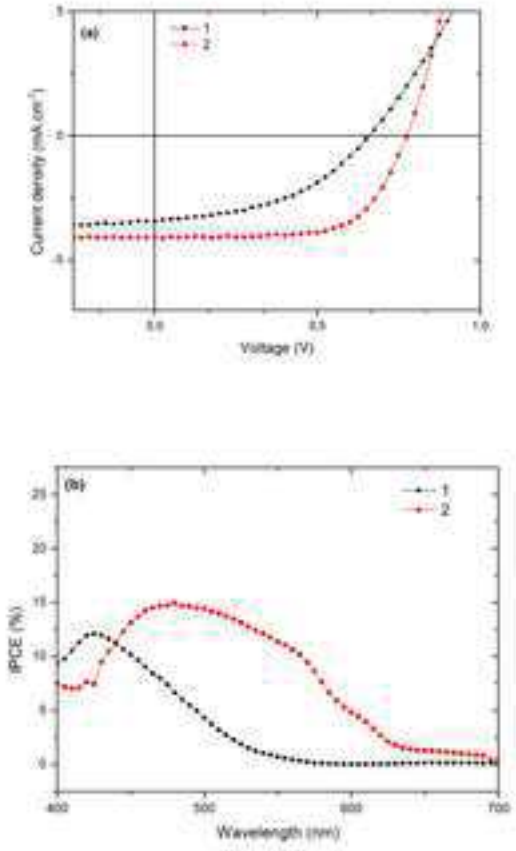

Figure 10. (a) Photocurrent density-voltage curves under illumination and (b) incident photon-to-current conversion efficiency (IPCE) spectra of **1**- and **2**-sensitized DSSCs.

This paper is elaborated at the Centre of Excellence in Advanced Material Research and Technology Transfer of the Institute of Solid State Physics, University of Latvia executing project CAMART² that has received funding from the Horizon 2020 Framework Programme H2020-WIDESPREAD-01-2016-2017-TeamingPhase2 under grant agreement No. 739508